


Article

Assessing Radiometric Stability of the 17-Plus-Year TRMM Microwave Imager 1B11 Version-8 (GPM05) Brightness Temperature Product

Ruiyao Chen ^{1,*}, Faisal Alquaied ²  and W. Linwood Jones ¹

¹ Department of Electrical and Commuter Engineering, University of Central Florida, Orlando, FL 32816, USA; wlinwoodjones@gmail.com

² King Abdulaziz City for Science and Technology, Riyadh 11442, Saudi Arabia; mstthmr@gmail.com

* Correspondence: chenruiyao@gmail.com; Tel.: +1-407-435-8328

Received: 31 October 2017; Accepted: 5 December 2017; Published: 7 December 2017

Abstract: The NASA Tropical Rainfall Measuring Mission (TRMM) Microwave Imager (TMI) has produced a 17-plus-year time-series of calibrated microwave radiances that have remarkable value for investigating the effects of the Earth's climate change over the tropics. Recently, the Global Precipitation Measurement (GPM) Inter-Satellite Radiometric Calibration (XCAL) Working Group have performed various calibration and corrections that yielded the legacy TMI 1B11 Version 8 (also called GPM05) brightness temperature product, which will be released in late 2017 by the NASA Precipitation Processing System. Since TMI served as the radiometric transfer standard for the TRMM constellation microwave radiometer sensors, it is important to document its accuracy. In this paper, the various improvements applied to TMI 1B11 V8 are summarized, and the radiometric calibration stability is evaluated by comparisons with a radiative transfer model and by XCAL evaluations with the Global Precipitation Measuring Microwave Imager during their 13-month overlap period. Evaluation methods will be described and results will be presented, which demonstrate that TMI has achieved a radiometric stability level of a few deciKelvin over almost two decades.

Keywords: TRMM; radiometric stability; TMI 1B11 V8 (GPM05); inter-satellite calibration

1. Introduction

The Tropical Rainfall Measuring Mission (TRMM) was a joint space project between the National Aeronautics and Space Administration (NASA) and the Japanese Aerospace Exploration Agency (JAXA) to measure tropical precipitation from a low-inclination orbit [1]. It was launched in November 1997, into a near circular non-sun-synchronous orbit with an inclination of 35° and at an altitude of 350 km, which was later boosted to 403 km in 2001. After providing important rainfall measurements of tropical precipitation for 17 years, the system was decommissioned on 15 April 2015, when the spacecraft depleted its fuel that was required for orbit maintenance.

For TRMM, the primary instruments for measuring rainfall were microwave, namely: the passive TRMM Microwave Imager (TMI), and the active Precipitation Radar (PR), while this paper focuses on only the TMI radiometric calibration characteristics over this 17-year legacy period. For the TRMM constellation of cooperative satellites, the TRMM Project used a common rain retrieval algorithm (GPROF), which assumed all the radiometer sensors were radiometrically intercalibrated. For this purpose, TMI was used as the radiometric transfer standard to perform inter-satellite radiometric cross-calibration (XCAL) of the constellation, until it was decommissioned.

For TMI to serve as the radiometric transfer standard, it was necessary to carefully assess the calibration accuracy and stability of this instrument, which is the goal of this paper. Previous to this research, there was an evolutionary development of the algorithm to process TMI sensor data to yield

the desired earth scene brightness temperature (T_b) that resulted in several versions (V6 and V7) of the TMI 1B11 brightness data product [2,3], which were largely based on a number of empirical ad-hoc corrections. To produce the legacy TMI T_b product, known as 1B11 Version-8 (V8) or GPM05, a new algorithm based on rigorous physical principles and on-orbit measurements over the entire 17-plus-year history of TMI measurements was developed. During this process, several important discoveries were made and corrections were implemented to mitigate these instrument anomalies.

The Global Precipitation Measurement (GPM) mission launched in February 2014 will continue the legacy of TRMM to provide the next generation of global measurements of precipitation from space [4]. The GPM observatory also carries a multi-frequency microwave imager named the GPM Microwave Imager (GMI). The GMI on-orbit radiometric performance has been demonstrated to be excellent [5,6]; therefore, it is the new calibration standard reference to which the TMI brightness temperature (T_b) datasets were inter-calibrated during their 13-month overlap period from March 2014 to March 2015.

2. Materials and Methods

2.1. TMI 1B11 V8 (GPM05)

2.1.1. Algorithm Development

In this section, the changes of the final legacy TMI product will be described. The purpose of these changes are to make the final revision more robust than previous versions that were based on ad-hoc corrections. The main modifications in the final version are the following: TRMM's geolocation correction, scan bias correction, reducing the effect of the noise equivalent delta- T_b (NEDT), Radio Frequency Interference (RFI) in the Cold Sky Reflector (CSR) correction, hot load correction, and the Main Reflector (MR) emissive antenna correction.

The first change in 1B11 V8 is the geolocation calculation, which provides the geodetic latitude and longitude for each observation, has been improved. There are three components that are responsible for the geolocation data: TRMM orbit ephemeris, TRMM attitude and TMI's antenna pointing alignment. The ephemeris information, which includes the Greenwich Hour Angle (GHA), was provided by the NASA Goddard Space Flight Center (GSFC), and some errors in the ephemeris GHA were identified in 2013. These errors have been corrected in V8 by using the latest information from the U.S. Naval Observatory. The geolocation accuracy after correcting the ephemeris increased to 0.1 km instead of 0.45 km from previous versions [7].

In previous versions, errors were identified in the spacecraft attitude for yaw and roll, which were subsequently corrected based on the PR measurements [8]. The correction was only applied from the beginning of the mission to 15 January 2010. For V8, the spacecraft attitude was recomputed using new ground-definitive attitude computation software that uses spacecraft gyro and sun sensor data along with the measurements of the spacecraft roll derived using the PR science data for the entire mission. The V8 attitudes improve the accuracy from tenths of a degree range to hundredths of a degree range [7].

Furthermore, the TMI antenna boresight pointing offset (spin axis misalignment) was reanalyzed in V8 for each channel. The nominal value of the antenna boresight offset from the spin axis was 49° for all channels. However, better values were found for each feed horn: 49.45° for the 10 GHz feed horn and 49.28° for the high-frequency feed horns. In addition, the 10 GHz feed horn showed different value for each polarization: 49.4° for the vertical (V-pol) polarization and 49.5° for the horizontal polarization (H-pol). Moreover, the starting azimuth angle for observations was found to be -63.91° for the 10 GHz feed horn and -64.36° for the high-frequency feed horns. Since the 10 GHz feed horn was directed to the main reflector earlier than the other feed horn, it was estimated to make its observations ahead by about 0.2 s. Finally, an overall alignment offset relative to TRMM spacecraft inertial coordinate system axes was estimated as -0.08° in pitch angle and 0.08° in roll [7,9].

The second main change applied to V8 was the scan Tb bias correction. In 2001, a Tb bias was found that was dependent upon the azimuth scan position, and it was reported that this bias also changed, based on the scene temperature [2]. However, in V7, the bias temperature was calculated for each channel based on the average ocean temperature. This was changed in V8, when the scan bias correction was updated to be dependent on the scene temperature, as seen in Figure 1 [9].

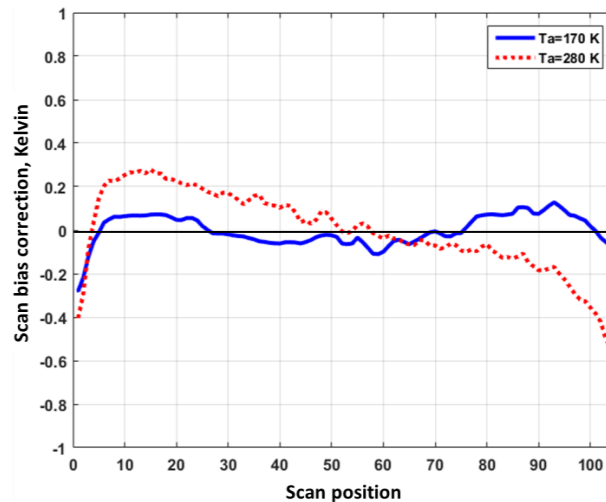


Figure 1. Scan bias correction for channel 10.65 V for $T_a = 170$ K (blue solid line) and $T_a = 280$ K (red dashed line).

The third improvement in V8 was to average hot and cold load calibration samples from consecutive scans to reduce the effect of the NEDT during the calibration process. The true gain and offset should vary slowly on-orbit with changes in the physical temperature of the receiver. Based upon an analysis of the on-orbit receiver gain, it was determined that the gain was stable over a period of 20 s. Thus, an algorithm was implemented that uses a running average of 9 scans (current scan plus 4 scans backward and forward) for the hot load measured temperature (T_h), the hot load counts (Ch), and the cold counts (C_c) to compute the gain and offset [7]. In Figure 2, the calculated gain is shown with and without the scan averaged algorithm.

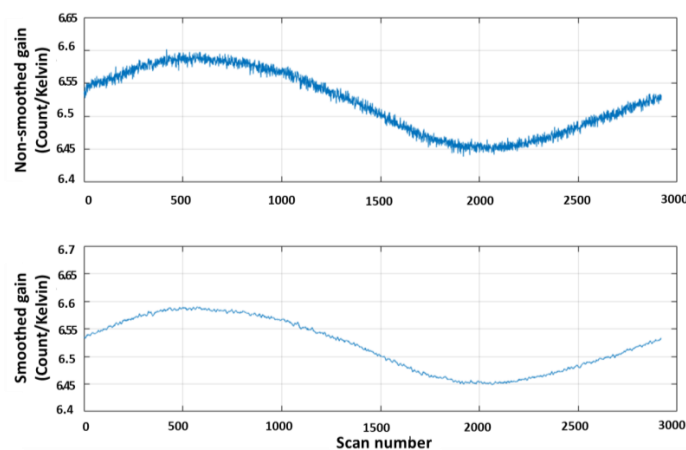


Figure 2. Smoothed (bottom panel) and non-smoothed (upper panel) calculated gain for channel 10.65 V and orbit # 92412.

The fourth modification in the final version was based on identifying and removing RFI in the cold counts. It was reported in [10,11] that there was an RFI intrusion coming from a geostationary

satellite through the CSR. This led to an increase in the cold count observations, which corrupted the calibration process and associated errors in the scene brightness temperatures. Thus, in V8, an algorithm was implemented that compares along-scan and cross-scan gradients to the normal maximums and determines the calibration state of the scan by combining the two results. Therefore, if a scan is flagged as RFI, the algorithm looks forward and backward to find nearest valid scans to apply a linear interpolation. This algorithm uses previous and post orbits to perform the calibration near orbit boundaries. Figure 3 demonstrates the effectiveness of the TRMM V8 processing, by comparing the scan mean cold load counts with or without corrections [7].

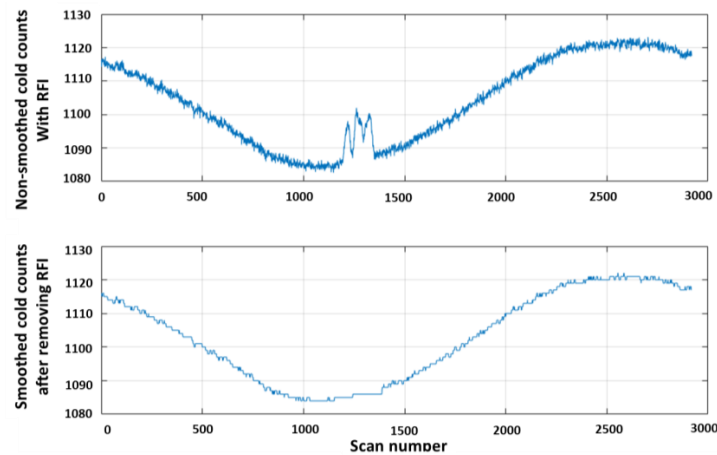


Figure 3. Cold counts with (**bottom panel**) and without (**upper panel**) Radio Frequency Interference (RFI) correction for channel 19.35 H and orbit # 87738.

The fifth change in V8 was to identify and correct the solar intrusion in the hot load counts. During the reprocessing of the TMI data, it was discovered that under certain solar geometry conditions, the radiometer hot counts (C_h) did not follow the measured hot load physical temperature (T_h) as expected, which indicated that there was a radiometric calibration anomaly associated with the hot load. To illustrate this effect, consider Figure 4 that shows a time series of TMI C_h , T_h , C_c (cold counts), calculated forward-transfer function gain and calculated forward-transfer function intercept in panel (a) to (e) respectively, for one orbital solar cycle (expressed as phase from orbit midnight). Therefore, a hot load correction procedure was developed and applied in 1B11 V8 that resulted in several lookup tables for each channel of the hot load physical temperature corrections (ΔTh) that were based on solar coordinates for different solar array orientations and two different spacecraft yaw values (yaw 0 and 180). For example, Figure 5 shows the hot load correction look-up table for channel 10.65, V-pol during the post-boost time [12]. In addition, Figure 6 shows the calculated gain with or without the hot load correction.

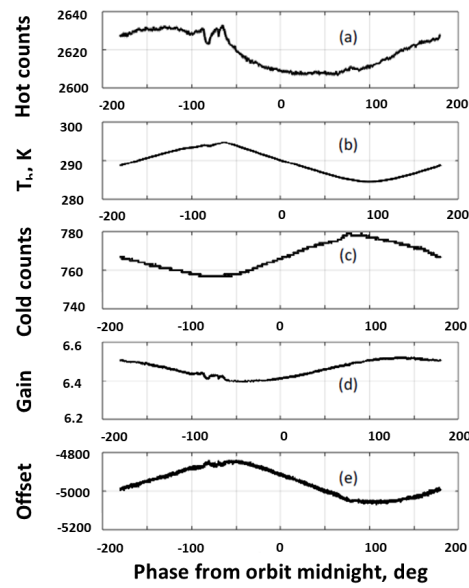


Figure 4. TMI parameters for 10.65 V channel during TRMM orbit # 87736: (a) hot counts, (b) measured hot load physical temperature, (c) cold counts, (d) receiver gain and (e) receiver offset.

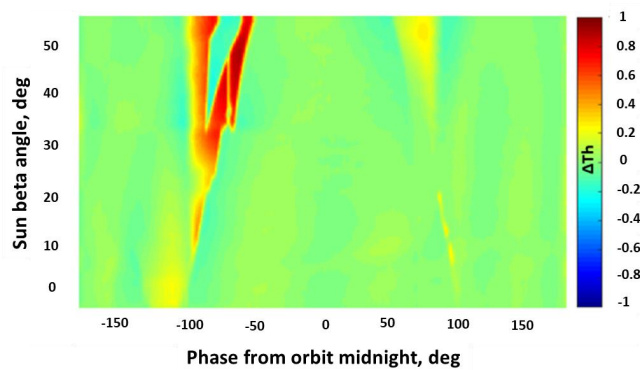


Figure 5. The hot load correction table for channel 10.65 V at yaw 0°, during the post-boost time.

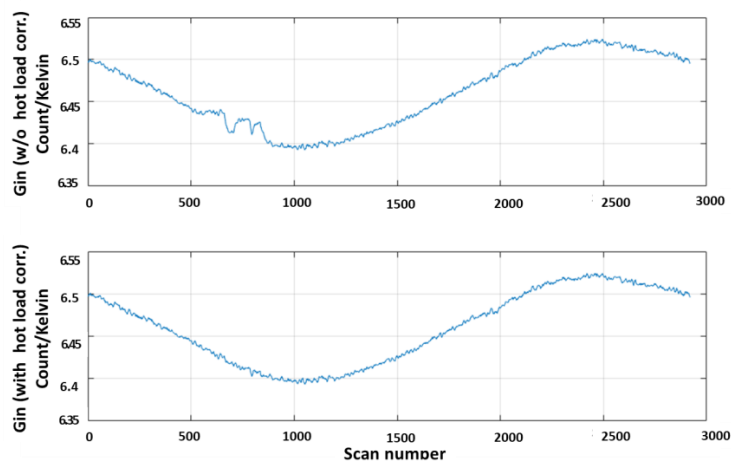


Figure 6. The calculated gain for channel 10.65 V with (bottom panel) and without (upper panel) hot load correction (orbit #87736).

The last major change was the MR emissive antenna correction. From the beginning of the mission, it was discovered that TMI Tb observations were warmer than expected for ocean scenes because of a slightly emissive MR. In 2001, Wentz et al. [2] developed a constant emissive MR correction, which was implemented in 1B11 V6, to remove the orbit-mean Tb bias, which was based on intersatellite comparisons with the Special Sensor Microwave Imager (SSM/I). However, 1B11 V6 was flawed in that a residual time-variable calibration bias remained due to the changing of the MR physical temperature. In 2006, 1B11 V7 was released after removing the dependency of the orbit physical temperature by using a lookup table that was based on solar beta angle and time since eclipse [3]. In the legacy 1B11 V8, which will be released at the end of 2017, the reflector emissivity coefficients for all TMI channels were measured during four deep space maneuvers conducted in 2015; and the reflector physical temperatures were derived for the entire 17-plus-year period based upon the single differences (SD) between the observed and theoretical brightness temperatures. Based upon these measurements and rigorous radiative transfer theory, the emissive reflector correction achieves a satisfactory brightness temperature correction stability of $<\pm 0.1$ K. Fortunately, the reflector orbital temperature cycle was quite repeatable with the deterministic solar coordinates; and as a result, four reflector physical temperature lookup tables were constructed for fixed spacecraft configurations (spacecraft yaw: $= 0^\circ$ and $= 180^\circ$, orbit altitudes: 350 km and 403 km) that cover the lifetime of TMI. For example, Figure 7 shows the MR physical temperature lookup table for yaw 0° and altitude 403 km. This robust emissivity correction algorithm yielded a high quality 1B11 V8 product to replace the previous V7 that was based upon a number of ad-hoc radiometric calibration corrections [13].

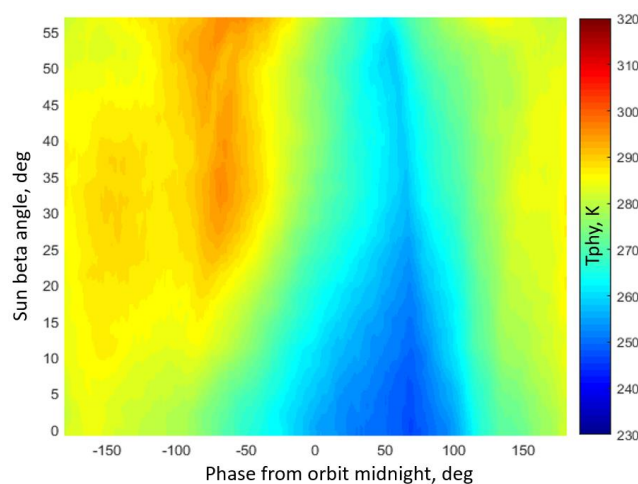


Figure 7. TMI's Main Reflector physical temperature (yaw 0° and post-boost altitude = 403 km).

2.1.2. Importance of the Stability Assessment

Since the TRMM constellation have provided almost two decades of calibrated microwave radiances, these observations have great potential for use in climate studies. However, this requires a very strict inter-satellite radiometric calibration between sensors to assure consistent environmental parameter retrievals. Thus, the GPM inter-satellite radiometric calibration working group (XCAL) was formed and charged with the responsibility of developing robust techniques to preform and maintain the radiometric calibration of constellation radiometer instruments, relative to one another. Because TRMM's orbit was non-sun-synchronous, it had frequent near-simultaneous collocations with the other radiometers in polar orbits, therefore it was selected as the radiometric transfer standard for the constellation. Thus, by having a standard calibration for all these instruments, the global brightness temperature dataset was unified [14].

Moreover, for TMI to serve as the radiometric transfer standard, it was necessary to carefully assess the calibration accuracy and stability of this instrument. Over the TRMM mission, there have

been several versions of the TMI brightness temperature products 1B11, which have been evolutionary developments that included a number of ad-hoc corrections. Therefore, the new version, 1B11 V8 produced from this final “legacy” processing of the TMI brightness temperatures needs to be carefully inspected before being released to the science community for further research.

2.2. Approaches

After applying the 1B11 V8 algorithm described in Section 2.1, the brightness temperatures have been validated by two methods. First, the simulated (modeled) brightness temperatures were used to calculate the SD between the observed and the modeled, which is a good indication of the stability of the Tb measurements. For example, SD’s that do not change in time are sufficient to assure a stable radiometric calibration. However, the contrary may not necessarily indicate calibration instability because this SD method is sensitive to uncertainty in the input environmental parameters for atmosphere and surface, as well as issues with the physics of the RTM used to produce the modeled Tb’s. Another method, which is more robust, was to use inter-satellite radiometric calibration to calculate the double difference (DD) between TMI and another well calibrated instrument (GMI). This DD method dramatically reduces the issues associated with the SD technique; however, it uses less points, because it depends on the collocation between two instruments.

2.2.1. Single Differences

Since TMI operated for more than 17 years, the observed Tb stability is an important metric to be evaluated. Therefore, the SD between the observed and simulated Tb over more than 15 years are analyzed as an indicator of its long-term radiometric stability. The simulated Tb was obtained using the XCAL ocean RTM. In this paper, the Remote Sensing Systems (RSS) surface emissivity model [15,16], the Rosencrantz atmospheric water vapor absorption model [17,18] and the Liebe atmospheric oxygen absorption model were combined to form the XCAL RTM [15–19]. The radiometer parameter inputs were: the channel frequency, the earth incidence angle (EIA), and the polarization (V- and H-pol). The environmental dataset was from the Global Data Assimilation System (GDAS), which uses NOAA’s Global Forecast System (GFS) model (NCEP 2000) to provide outputs at 0000, 0600, 1200, and 1800 Greenwich Mean Time (GMT), on a $1^\circ \times 1^\circ$ latitude (lat)/longitude (lng) grid [20].

The procedure used to calculate the single differences between TMI observed and simulated Tb is shown in Figure 8. The collocation process for TMI Tb’s and the environment parameters of GDAS was performed in $1^\circ \times 1^\circ$ latitude (lat)/longitude (lng) boxes. Within each 1° box, the Tb’s were combined, and the means and standard deviations were calculated. Afterwards the observed mean Tb’s were compared with the simulated Tb for that box. Since the GDAS model output is available every 6 h, a ± 2 h window for collocations that occurred 4 times per day was used.

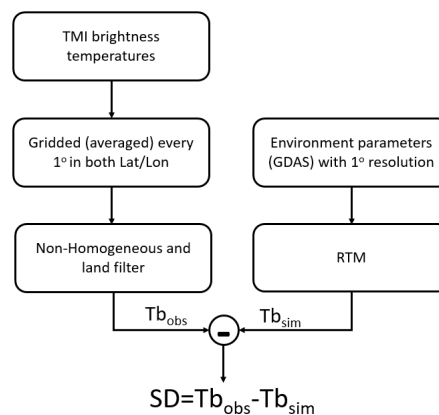


Figure 8. Flow chart for Single Differences procedure, between observed and modeled brightness temperature.

The SD procedure seeks to estimate long-term Tb biases between radiometers, therefore, it is important that the collocations be carefully filtered to provide only high quality data for comparisons. The ideal conditions are homogeneous clear-sky ocean conditions, where there is the greatest confidence in the simulated Tb's. As a result, the match-up dataset was subject to conservative filters, which typically reduce SD comparisons to <50% of the possible collocations. An effective filter used was the standard deviation test, which removes non-homogeneous environmental conditions that include heavy clouds, rain, and mixed ocean/land scenes [21]. Cloud liquid water from GDAS was also used to as a filter to ensure cloud-free ocean scene. Finally, a filter based upon a threshold of the maximum observed ocean Tb by channel was also used.

Then, the SD's for each channel were obtained by:

$$SD_{TMI} = T_{b-obs} - T_{b-sim} \quad (1)$$

2.2.2. Double Differences

Because the GDAS data is only an estimate of the true environmental conditions and the ± 2 -h collocation time window is relatively large for environmental parameter stability, it is desirable to use another well calibrated instrument with relatively high temporal resolution for validation and calibration. The GMI instrument has been carefully vetted and found to be an extremely well calibrated microwave radiometer. As a result, the radiometric intercalibration of TMI to GMI serves to provide a common radiometric calibration for other radiometers that existed previously during the TRMM era. Therefore, the intercalibration between TMI and GMI was performed using the three versions of TMI products: V6, V7 and the new V8.

Because of differences in frequency and EIA between the two radiometers, as shown in Table 1, the direct comparison between their observed brightness temperatures does not reflect the true instrument Tb bias of one to the other. However, using the difference between the SD's of the two instruments, which is the DD, is a robust technique for establishing the calibration bias [21]:

$$DD = SD_{target} - SD_{reference} \quad (2)$$

where the reference is the well calibrated instrument (GMI) and the target is TMI.

Table 1. Center frequency and earth incidence angle (EIA) of TMI and GMI channels.

TMI		GMI	
Freq (GHz)	EIA (deg)	Freq (GHz)	EIA (deg)
10.65 V/H	53.5/53.6	10.65 V/H	52.8
19.35 V/H	53.4	18.70 V/H	52.8
21.30 V	53.4	23.80 V	52.8
37.00 V/H	53.4	36.64 V/H	52.8
85.50 V/H	53.4	89.00 V/H	52.8

Since the resolution of the SD is a 1° box in latitude and longitude, the DD resolution will be the same. To improve the quality of the intercalibration, any match-ups with time difference more than ± 1 h were removed. Moreover, the standard deviation of the DD values is indicative of the radiometric stability, and the mean DD will be used to calibrate TMI to match GMI. Ideally, the DD biases should be a constant; however, results show some correlation with the yaw orientation, orbital latitude, solar coordinates and scene temperature, which will be discussed next.

3. Results

3.1. Single Differences

The SD for channel 10.65 V are plotted in Figure 9, where the values are averaged by bin and are separated by yaw orientation (yaw 0 and 180 degrees) for each quarter year. This channel is the most important because the main reflector physical temperatures were derived based on this channel. During the over 15-year time series, from 2000 to the end of the mission, these results show amazing stability, where the time series is flat with a mean <0.01 K and a standard deviation <0.07 K for both yaw orientations. This result is very sufficient to verify that this channel is extremely stable because it is highly unlikely that both the observed Tb and the modeled Tb can vary in synchronism to cancel.

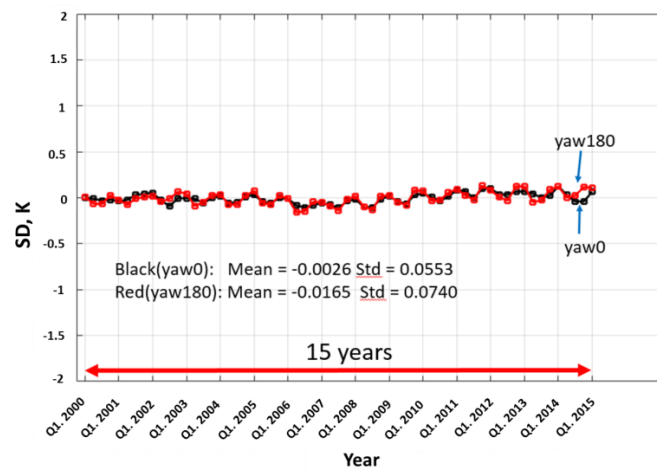


Figure 9. Single differences (SD) quarterly results for both orientations (yaw 0° in black and 180° in red) for 15 years (channel 10.65 V).

3.2. Double Differences

3.2.1. Comparison between V8 and V6/V7

The TMI/GMI DD distributions for channel 10.65 V for V6, V7, and V8 are shown in Figure 10. Consider first the V6 histogram, shown in red, where the major change was to remove the mean emissive antenna bias. This bias adjustment was based on an ad-hoc procedure involving several months of inter-satellite comparisons, but the MR physical temperature was incorrectly assumed to be constant. Thus, the orbital cycle of MR physical temperature produced a time-varying radiometric calibration error in the earth scene brightness temperature that resulted in the large histogram variance.

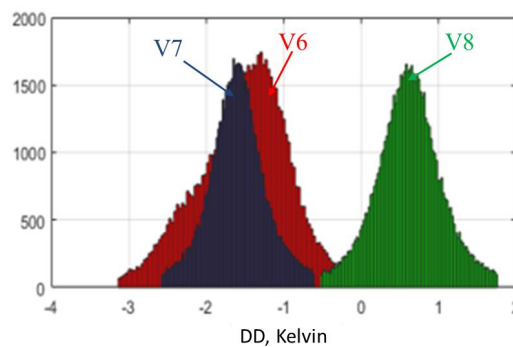


Figure 10. Double Differences (DD) distribution of channel 10.65 V for 1B11 V6 (red), V7 (blue) and V8 (green).

Next, consider the V7 histogram, shown in blue in Figure 10. This version was an addition to version 6 that removed the effects of the orbital cycle of the MR physical temperature. Thus, the histogram mean was similar to V6 but the variance was significantly reduced. In addition, the basis of the emissive reflector correction were empirical comparisons with theoretical brightness temperatures provided by a RTM.

Finally, V8 was developed based upon rigorous physical measurements and electromagnet theory, as described in the preceding section. This is a very important improvement over V7, because the long-time series of Tb observations have magnificent application in earth science for the study of global climate change. The credibility of the brightness temperature calibration is an important factor in the utility of the experimental data, and V8 is superior to all previous versions. Concerning the DD histograms, except for the difference in the mean value, V7 and V8 are closely resembling. This means that V7 provided an excellent Tb product, but it lacked credibility because it was based upon ad-hoc methods. Further, there is no significance to V8 bias being less than V7; rather it is only necessary that the mean value be accurately known. Similar results were also observed in all the other eight channels.

3.2.2. Stratification of DD

One metric for the DD biases, is the stability of the mean value when data are sorted in various ways. Besides using GDAS as environmental data to derive DD biases, another dataset called European Centre for Medium-Range Weather Forecasts (ECMWF) Reanalysis Interim (ERA-I) [22] was also used to increase our confidence in the results. Therefore, four cases of radiometric intercalibration of TMI relative to GMI are implemented to evaluate the TMI V8 dataset with respect to V7. Case 1 refers to the intercalibration of TMI V7 relative to GMI, using GDAS as ancillary data. Case 2 is also TMI V7 but with ERA-I. Case 3 is TMI V8 with GDAS, and Case 4 is TMI V8 with ERA-I. The mean and standard deviation (STD) values of DD's over the 13-month period of all the channels are listed in Table 2. The results between using GDAS and ERA-I are extremely close to each other (Case 1 compared to Case 2, and Case 3 compared to Case 4). When Case 1 is compared to Case 3 or Case 2 compared to Case 4, it is noticeable that the average values of DD's changed from V7 to V8. The minimum change is 0.8 K for the 89 GHz H-pol and the maximum is 2.41 K for the 10 GHz V-pol. The STD values changed slightly from V7 to V8, where 19 GHz V- and H-pol have the maximum changes, ≥ 0.1 K.

Table 2. Double Differences Mean and STD.

		10V	10H	19V	19H	23V	37V	37H	89V	89H
CASE 1	V7, GDAS	-1.21/	-1.69/	0.67/	0.16/	-0.07/	-2.15/	-0.83/	-1.25/	-1.32/
		0.29 *	0.30	0.54	0.71	0.57	0.46	0.66	0.40	0.67
CASE 2	V7, ERA-I	-1.21/	-1.70/	0.72/	0.27/	0.04/	-2.16/	-0.85/	-1.20/	-1.32/
		0.29	0.31	0.58	0.81	0.61	0.48	0.69	0.42	0.73
CASE 3	V8, GDAS	0.64/	0.72/	0.37/	1.30/	1.01/	-0.79/	1.01/	0.32/	-0.55/
		0.26	0.29	0.43	0.57	0.50	0.44	0.68	0.40	0.67
CASE 4	V8, ERA-I	0.63/	0.71/	0.42/	1.41/	1.13/	-0.80/	1.02/	0.34/	-0.53/
		0.27	0.3	0.48	0.69	0.54	0.46	0.71	0.42	0.73
	$\langle Tb_{scene} \rangle$	170.2	92.1	195.8	130.1	228.6	217.1	156.9	267.5	240.7

* x/y: x is Mean, and y is STD of double differences. $\langle Tb_{scene} \rangle$ is the scene temperature of GMI.

The monthly DD's of the four cases are presented in Figure 11, in which the DD's barely vary with the different environmental datasets. All the four cases show very small monthly dependence; however, V7 DD's are relatively less stable than those of V8 for the 19V, 19H and 23V channels.

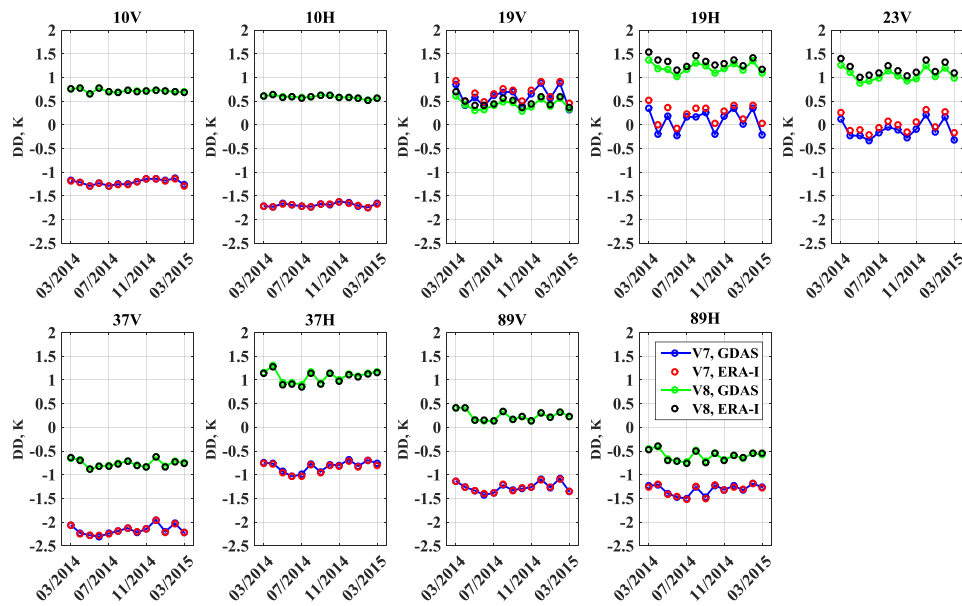


Figure 11. Monthly intercalibration double differences (DD) for TMI relative to GMI for four cases. Red line indicates monthly averaged DD using TMI V7 Tb and GDAS environmental data; blue is TMI V7 but with ERA-I; green is TMI V8 with GDAS and black is TMI V8 but with ERA-I data.

Ideally, when the DD’s are separated into two yaw orientations, they should be identical. To examine this, the difference between DD_{yaw-0} and $DD_{yaw-180}$ are calculated and presented in Figure 12 for all the 9 channels. For both V7 & V8, the change in DD’s between the two yaw flips is small for all channels with largest difference being -0.4 K & -0.3 K respectively at 23 GHz V channel. For all channels, V8 appears to be <0.1 K smaller than V7.

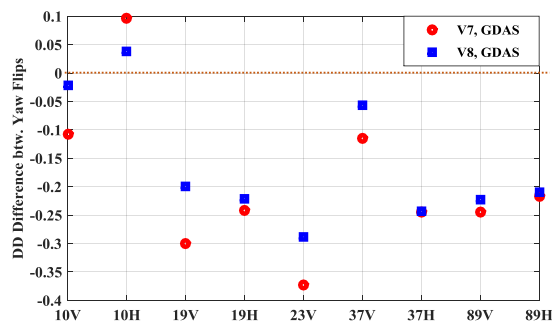


Figure 12. Mean double difference (DD) between Yaw 0° and 180° of each channel for both V7 (red dots) and V8 (blue squares).

Continuing the analysis (see Figure 13), it was noticed that the DD anomaly from V7 shows a systematic dependence, when sorted on latitude for the 19V, 19H and 23V channels. It is noted that similar results have been previously presented by Chen et al. [23]. While the reason for this is not fully understood, it is believed that this is related to the water vapor absorption line at 22 GHz; and moreover in V8, the DD latitude dependence is evidently improved.

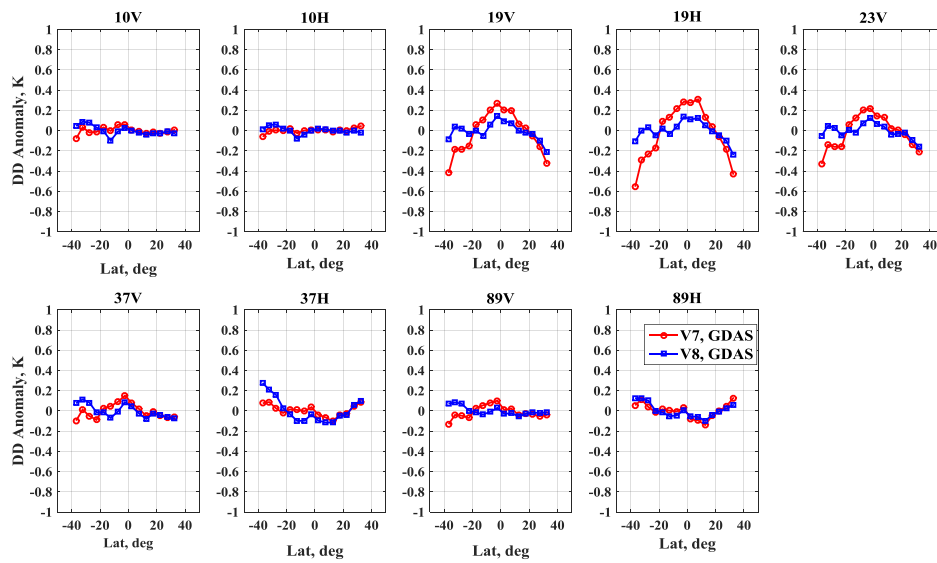


Figure 13. Comparison of latitude dependence of double difference (DD) anomaly for TMI V7 (red triangles) and V8 (green dots).

Since the correction of the emissive antenna and the sun intrusion to the hot load were based on the solar coordinates, it was important to assess the change in DD anomaly (CDDA) from V7 and V8 which is calculated as follows:

$$CDDA(\beta, \text{phase}) = (DD_8 - \langle DD_8 \rangle) - (DD_7 - \langle DD_7 \rangle) \tag{3}$$

where $\langle DD_7 \rangle$ and $\langle DD_8 \rangle$ are the averaged DD for V7 and V8 respectively. The resulting CDDA was stratified based on the solar coordinates, which are the sun beta angle and the phase from orbit midnight. The scattered DD for channel 19.35 V and 0° yaw orientation is shown in Figure 14, which includes relatively large differences ($> \pm 0.4$ K), especially in the region of the solar intrusion into the hot load. This verifies the improvement of the hot load correction procedure.

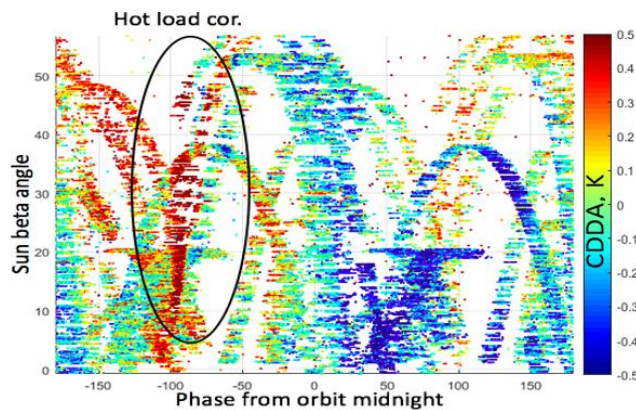


Figure 14. Change in DD anomaly (CDDA) from V7 to V8 based on the solar coordinates of channel 19.35 V.

Furthermore, a scatter plot between the GMI earth scene brightness temperatures and the values of $DD > \pm 0.4$ K at 19.35 GHz V channel is shown in Figure 15. It is apparent that V8 DD's appear to be independent of the scene brightness with a slope close to zero, while V7 DD's have a perceptible positive linear dependence with a slope of +0.04 K/K.

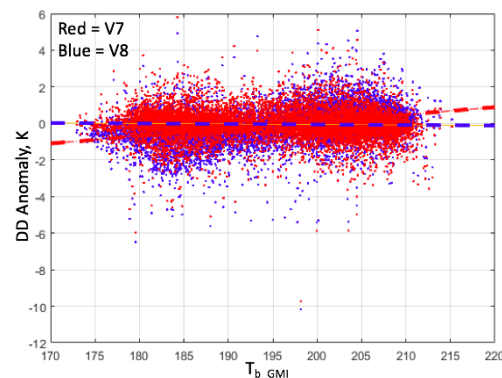


Figure 15. Correlation between double difference (DD) bias and the GMI earth scene brightness temperature for V7 (red) and V8 (blue) at channel 19.35 V

4. Discussion

The five major changes, which have been incorporated into an improved TMI radiometer Tb algorithm, are summarized in this article. Using this new algorithm, the entire >17-year time series has been reprocessed to produce the legacy 1B11 V8 brightness temperature product, which was used to perform inter-satellite XCAL with the other members of the TRMM constellation.

This paper documents the validation of the 1B11 V8 Tb product. The reprocessed Tb time series are compared to the theoretical (modeled) Tb from the XCAL RTM for >15-year period, and the single differences between them are calculated. A detailed analysis of results demonstrates that all 9-channels of the TMI exhibit extraordinarily long-term stability. Moreover, the V8 Tb are compared to the previous version, V7, by using the XCAL double difference technique with the GMI as the reference standard. Overall, TMI V8 dataset exhibits smaller DD biases with GMI, and the DD STD are slightly better. Moreover, for the 19V, 19H and 23V channels, the troublesome dependence on latitude that appears in TMI V7 is essentially removed in the V8 dataset. The V8 stability with time and yaw angle is also improved when compared to V7. Additionally, V7 DD has an apparent positive linear dependence on scene brightness that has been removed from V8.

Moreover, there is an increased confidence in this V8 data set as a climate data record, because of an improved pedigree that replaces ad-hoc radiometric calibrations (V6 and V7) by a rigorous derivation of radiometric uncertainty, based upon on-orbit measurements and electromagnetic theory. Therefore, this legacy brightness temperature product allows earth scientists to look for long-term changes in their earth geophysical models without fear of drifts in the TMI radiometric calibration.

Acknowledgments: This work was sponsored under a grant NNX16AE35G with the NASA Headquarters Earth Sciences Division for the Precipitation Measurement Mission. No funds have been allocated for publishing in open access.

Author Contributions: Ruiyao Chen and Faisal Alquaied performed this data analysis as PhD student research assistants under the guidance of their advisor W. Linwood Jones. The manuscript was prepared by Ruiyao Chen and Faisal Alquaied with suggestions and corrections from W. Linwood Jones. All authors have seen and approved the final article.

Conflicts of Interest: The authors declare no conflict of interest.

References

1. NASA Goddard Space Flight Center. Available online: http://trmm-fc.gsfc.nasa.gov/trmm_gv/information/brochure/brochure.html (accessed on 15 January 2015).
2. Wentz, F.J.; Ashcroft, P.; Gentemann, C. Post-launch calibration of the TRMM microwave imager. *IEEE Trans. Geosci. Remote Sens.* **2001**, *39*, 415–422. [[CrossRef](#)]
3. Gopalan, K.; Jones, W.L.; Biswas, S.; Blanow, S.; Wilheit, T.; Kasparis, T. A Time-Varying Radiometric Bias Correction for the TRMM Microwave Imager. *IEEE Trans. Geosci. Remote Sens.* **2009**, *47*, 3722–3730. [[CrossRef](#)]

4. Skofronick-Jackson, G.; Petersen, W.A.; Hou, A.Y.; Stocher, E.F.; Kaye, J.; Kakar, R. GPM Science Implementation Plan. Available online: <http://pmm.nasa.gov/category/document-type/science-implementation-plans> (accessed on 6 March 2015).
5. Draper, D.W.; Newell, D.A.; Wentz, F.J.; Krimchansky, S.; Skofronick-Jackson, G.M. The Global Precipitation Measurement (GPM) Microwave Imager (GMI): Instrument overview and early on-orbit performance. *IEEE Trans. Geosci. Remote Sens.* **2015**, *8*, 3452–3462.
6. Chen, R.; Ebrahimi, H.; Jones, W.L. Three-way inter-satellite radiometric calibration between GMI, TMI and WindSat. In Proceedings of the 2016 IEEE International Geoscience and Remote Sensing Symposium (IGARSS), Beijing, China, 10–15 July 2016; pp. 2036–2039.
7. Stocker, E.F.; Alquaied, F.; Bilanow, S.; Ji, Y.; Jones, W.L. TRMM Version 8 reprocessing improvements and data suite. *J. Atmos. Ocean. Technol.* **2017**, in press.
8. Bilanow, S.; Slojkowski, S. TRMM on-orbit performance reassessed after control change. In Proceedings of the International Symposium on Space Technology and Science, Kanazawa, Japan, 4–11 June 2006; pp. 528–537.
9. Kroodsma, R.; Bilanow, S.; Ji, Y.; McKague, D. TRMM Microwave Imager (TMI) Updates for Final Data Version Release. In Proceedings of the 2017 IEEE International Geoscience and Remote Sensing (IGARSS), Fort Worth, TX, USA, 23–28 July 2017.
10. Wentz, F.J. A 17-yr climate record of environmental parameters derived from the Tropical Rainfall Measuring Mission (TRMM) Microwave Imager. *J. Clim.* **2015**, *28*, 6882–6902. [[CrossRef](#)]
11. Farrar, S.; Jones, L. Corruption of the TRMM microwave imager cold sky mirror due to RFI. In Proceedings of the 2016 14th Specialist Meeting on Microwave Radiometry and Remote Sensing of the Environment (MicroRad), Espoo, Finland, 11–14 April 2016; pp. 76–81.
12. Alquaied, F.; Chen, R.; Jones, L. Hot Load Temperature Correction for TRMM Microwave Imager in the Legacy Brightness Temperature. *IEEE J. Sel. Top. Appl. Earth Obs. Remote Sens.* **2017**, in press.
13. Alquaied, F.; Chen, R.; Jones, L. Emissive Reflector Correction in the Legacy Version 1B11 V8 (GPM05) Brightness Temperature of the TRMM Microwave Imager. *IEEE J. Sel. Top. Appl. Earth Obs. Remote Sens.* **2017**, in press.
14. Wilheit, T.T. Comparing calibrations of similar conically scanning window-channel microwave radiometers. *IEEE Trans. Geosci. Remote Sens.* **2013**, *51*, 1453–1464. [[CrossRef](#)]
15. Meissner, T.; Wentz, F.J. The complex dielectric constant of pure and sea water from microwave satellite observations. *IEEE Trans. Geosci. Remote Sens.* **2004**, *42*, 1836–1849. [[CrossRef](#)]
16. Meissner, T.; Wentz, F.J. The emissivity of the ocean surface between 6 and 90 GHz over a large range of wind speeds and earth incidence angles. *IEEE Trans. Geosci. Remote Sens.* **2012**, *50*, 3004–3026. [[CrossRef](#)]
17. Rosenkranz, P. Absorption of microwaves by atmospheric gases. In *Atmospheric Remote Sensing by Microwave Radiometry*; Janssen, M.A., Ed.; John Wiley and Sons: Hoboken, NJ, USA, 1993; p. 37.
18. Rosenkranz, P.W. Water vapor microwave continuum absorption: A comparison of measurements and models. *Radio Sci.* **1998**, *33*, 919–928. [[CrossRef](#)]
19. Liebe, H.; Rosenkranz, P.; Hufford, G. Atmospheric 60-GHz oxygen spectrum: New laboratory measurements and line parameters. *J. Quant. Spectrosc. Radiat. Transf.* **1992**, *48*, 629–643. [[CrossRef](#)]
20. NCEP FNL Operational Model Global Tropospheric Analyses. Available online: <https://rda.ucar.edu/datasets/ds083.2/> (accessed on 12 April 2016).
21. Biswas, S.K.; Farrar, S.; Gopalan, K.; Santos-Garcia, A.; Jones, W.L.; Bilanow, S. Intercalibration of microwave radiometer brightness temperatures for the global precipitation measurement mission. *IEEE Trans. Geosci. Remote Sens.* **2013**, *51*, 1465–1477. [[CrossRef](#)]
22. Dee, D.P.; Uppala, S.M.; Simmons, A.J.; Berrisford, P.; Poli, P.; Kobayashi, S.; Andrae, U.; Balmaseda, M.A.; Balsamo, G.; Bauer, P.; et al. The ERA-Interim reanalysis: Configuration and performance of the data assimilation system. *Q. J. R. Meteorol. Soc.* **2011**, *137*, 553–597. [[CrossRef](#)]
23. Chen, R.; Alquaied, F.; Ebrahimi, H.; Jones, W.L. Radiometric Validation of the TRMM Microwave Imager 1B11 V8 Brightness Temperature Product. In Proceedings of the 2017 IEEE International Geoscience and Remote Sensing (IGARSS), Fort Worth, TX, USA, 23–28 July 2017.

